Battery Sizing of Small All-Electric Aircraft Using an Electro-Thermal Cell Model

1st Yawen Liang
ESE Department.
Delft University of Technology.
Delft, The Netherlands
y.liang-3@tudelft.nl

2nd Gautham Ram Chandra Mouli
ESE Department.
Delft University of Technology.
Delft, The Netherlands
g.r.chandramouli@tudelft.nl

3rd Pavol Bauer
ESE Department.
Delft University of Technology.
Delft, The Netherlands
p.bauer@tudelft.nl

2025 Energy Conversion Congress & Expo Europe (ECCE Europe) | 979-8-3315-6752-1/25/$31.00 ©2025 IEEE | DOI: 10.1109/ECCE-EUROPE62795.2025.11238666

***Abstract*—Electric aircraft represent a promising low-emission alternative to conventional fuel-powered aviation. This study proposes a battery sizing method for small all-electric aircraft using an electro-thermal battery cell model, considering different flight segments based on a reference commercial aircraft. The experiment is conducted to verify the proposed electro-thermal battery cell model. It considers varying battery efficiency throughout the flight mission, highlighting the importance of battery efficieny in the design process.**

***Index Terms*—All-electric aircraft (AEA), battery, electro-thermal model, efficiency.**

I. Introduction

OVER the past decades, the rising consumption of fossil fuels and carbon emissions have highlighted the necessity for the adoption of electric aircraft (EA). Offering a cleaner alternative to conventional aircraft, EA not only reduces environmental impact but also operates with significantly less noise. Moreover, they achieve better aerodynamic efficiency during flight. Among the various types of aircraft, small all-electric aircraft (AEA) with limited range are anticipated to be particularly viable for electrification in the next decade, driven by ongoing advancements in battery technology [1], [2].

In the emerging field of AEA battery power and energy sizing, limited studies have been conducted. The study by [3] proposed an integrated approach to sizing small AEAs, derived from mission analysis through flight mechanics and design constraints from a sizing matrix, though it did not consider power and energy consumption during the takeoff phase. [4] utilized mathematical models to translate flight performance requirements into constraints for powertrain components and subsequently introduced an optimal design approach for small hybrid-electric aircraft aimed at minimizing takeoff weight. In [5], the AEA mission power profile, including takeoff, climb, cruise, descent, and reserve phases, was computed using estimated parameters based on historical data of current aircraft. The takeoff weight was defined using the typical empty weight fraction of current commercial fuel-based aircraft, serving as a constraint for this analysis. In [6], a battery sizing method that integrates all design requirements through an iterative approach was proposed. This method considers realistic specifications based on the reference aircraft, includes a detailed component-level weight analysis to determine takeoff weight, and incorporates an in-depth mission analysis.

Building on previous research, this paper presents an improved battery sizing methodology for small, short-range AEA utilizing an integrated electro-thermal battery model. The approach begins with the specifications and mission parameters of the reference commercial aircraft across different flight phases. These parameters are used to estimate the battery power output and AEA weight components, including battery pack, powertrain, and the takeoff weight, while accounting for the variable efficiency of the battery, which depends on state-of-charge (SOC), C-rate, and temperature. Existing sizing methods have not yet incorporated the varying battery efficiency. This gap is particularly significant for AEAs, as variations in battery efficiency directly influence energy consumption throughout the flight mission and overall weight, thus affecting the sizing result.

II. Electro-thermal battery cell model

To predict battery efficiency over the entire flight mission, an electro-thermal coupled model for the battery cell is established. This model consists of two interconnected submodels, as illustrated in Fig. 1. The electrical submodel predicts battery cell voltage, current, and SOC in response to the required battery power and cell temperature. The thermal submodel predicts the cell temperature based on the current, resistance, and ambient

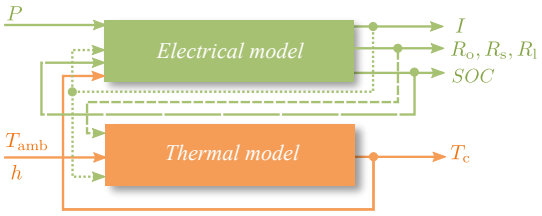

Fig. 1: Battery electro-thermal coupling model at the cell level.

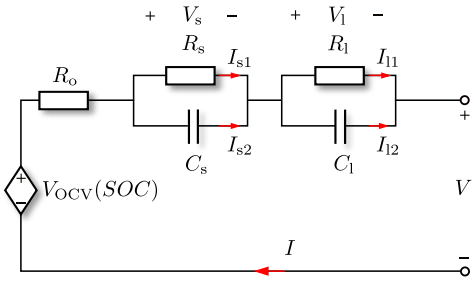

Fig. 2: Second-order RC Thévenin-based model.

temperature. For this study, it is assumed that all cells within the battery pack exhibit uniform behavior.

A. Electrical model at the cell level

In this study, the electric model adopts the second-order RC Thévenin-based model, as illustrated in Fig. 2. This model incorporates multiple components, including the open circuit voltage (OCV) V_{OCV}, the ohmic resistance R_{o}, the short-time transient parallel RC pair R_{s} and C_{s}, and the long-time transient parallel RC pair R_{l} and C_{l}. The equations for the electrical circuit model (ECM) discussed can be expressed as:

$$\begin{aligned} V_{\mathrm{l}}(t) &= I_{\mathrm{l1}}(t)R_{\mathrm{l}} = I(t)R_{\mathrm{l}}(1-e^{-\frac{t}{R_{\mathrm{l}}C_{\mathrm{l}}}}) \\ V_{\mathrm{s}}(t) &= I_{\mathrm{s1}}(t)R_{\mathrm{s}} = I(t)R_{\mathrm{s}}(1-e^{-\frac{t}{R_{\mathrm{s}}C_{\mathrm{s}}}}) \\ V(t) &= V_{\mathrm{OCV}}(t) - (V_{\mathrm{l}}(t) + V_{\mathrm{s}}(t) + I(t)R_{\mathrm{o}}) \\ I(t) &= \frac{P(t)}{V(t)} \\ SOC(t) &= \frac{\int I(t)dt}{S_{\mathrm{f}}} + SOC_0 \end{aligned} \tag{1}$$

where $I(t)$ is the battery cell current, which is split between the resistor current I_{s1} I_{l1} and the capacitor current I_{s2} I_{l2}. $V(t)$ is the terminal voltage of the battery cell. $P(t)$ is the battery cell power, which is determined by the operational requirements of the aircraft. S_{f} is the full battery capacity, and $SOC(t)$ is the real-time battery SOC. SOC_0 is the initial SOC.

TABLE I: Key parameters for the INR18650-35E battery.

Parameter	Value
Nominal capacity [A h]	3.4
Nominal voltage [V]	3.6
Charge operating temperature [°C]	0 to 45
Discharge operating temperature [°C]	-10 to 60
Gravimetric energy density [$\mathrm{W\,h\,kg^{-1}}$]	244.8
Weight [g]	50
Specific heat [$\mathrm{J\,kg^{-1}\,K^{-1}}$]	900

The ECM component values were determined using a pulse current test, following a methodology similar to that described in [7]. The OCV was determined using a similar pulse current test procedure. However, the resting period was extended to 3 h instead of 180 s to measure the close-to-equilibrium OCV. To extract the ECM parameters, the Samsung INR18650-35E cylindrical battery cell, which represents the NMC technology of LIBs, is chosen. This battery chemistry is expected to dominate air transportation in the near-term future due to its high energy density, well-established technology, and strong battery supply chain. The key parameters of the tested battery cell are outlined in Tab. I [8].

Due to the primary varying parameters during the AEA operation process, namely SOC, C-rate, and temperatures of the battery cell, the same test profile was repeated at different C-rate ranging from 0.2C to 1.0C and ambient temperatures, including $0°C$, $10°C$, $20°C$, $25°C$, $30°C$, and $40°C$, for three INR18650-35E cells. The ECM parameters for each operating condition were then extracted from the corresponding pulse test characterization results. Since the resistance value directly influences battery efficiency, the ECM resistance components at different temperatures are shown in Fig. 3. It can be observed that all resistance components increase at low SOC and low temperatures.

B. Thermal model at the cell level

1) Heat generation model and heat transfer model: The thermal model of the battery cell comprises the heat generation model and the heat transfer model. In this thermal model, the heat generation and temperature within the battery cell are assumed to be uniformly distributed [9]. According to the energy conservation law, the temperature change for a single battery cell can be expressed as follows:

$$m_{\mathrm{c}}C_{\mathrm{p,c}}\frac{dT_{\mathrm{c}}}{dt} = Q_{\mathrm{c}} - Q_{\mathrm{d}} \tag{2}$$

where m_{c} is the battery cell mass, $C_{\mathrm{p,c}}$ is the battery specific heat capacity at constant pressure. T_{c} is the

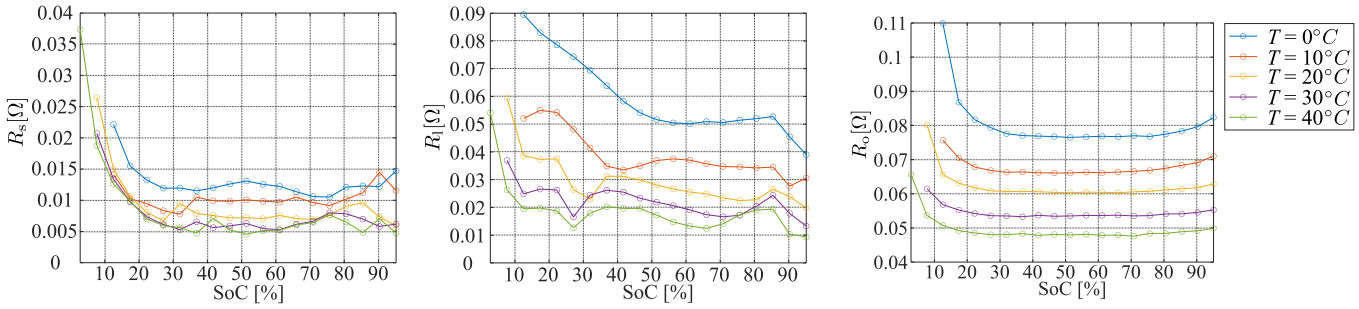

(a) R_s. (b) R_l. (c) R_o.

Fig. 3: ECM resistance variations with T under discharging process.

battery cell temperature. Q_c denotes the heat generation by a single battery cell, as defined in (3), and Q_d is the heat removed from the battery by the battery thermal management system (BTMS). The heat transfer process between the battery and the BTMS is described using Newton's law of cooling, as presented in (4).

$$\begin{aligned} Q_c &= Q_o + Q_p + Q_r \\ Q_o &= I^2 R_o \\ Q_p &= I_{s1}^2 R_s + I_{l1}^2 R_l \\ Q_r &= I T_c \cdot \frac{\partial V_{OCV}}{\partial T} \end{aligned} \tag{3}$$

$$Q_d = hS(T_c - T_{BTMS}) \tag{4}$$

where Q_o is the heat generation from ohmic resistance, Q_p is the heat generation from polarization resistance, and Q_r is reversible entropic heat. $\frac{\partial V_{OCV}}{\partial T}$ is the temperature rise coefficient of electromotive force. h is the heat transfer coefficient between the battery cell surface and the BTMS. T_{BTMS} is the BTMS temperature. S is the heat transfer surface area.

2) OCV and entropy coefficient: To characterize the temperature rise coefficient of electromotive force, the OCV test was conducted under different temperature conditions at $25°C$ and $40°C$ for different SOC. The measurement result is shown in Fig. 4. The entropy coefficient is defined as (5) [10].

$$\frac{\partial V_{OCV}}{\partial T}(SOC) = \frac{V_{OCV,T1} - V_{OCV,T2}}{T_1 - T_2} \tag{5}$$

where $V_{OCV,Tx}$ is the battery cell OCV measured at a certain battery cell temperature T_x. $\frac{\partial V_{OCV}}{\partial T}$ can be summarized as the function of SOC by polynomial fitting. Taking discharging as an example, the fitting expression is shown as:

$$\frac{\partial V_{OCV,dis}}{\partial T} = \sum_{i=1}^{7} d_{i,dis} SOC^{i-1} \tag{6}$$

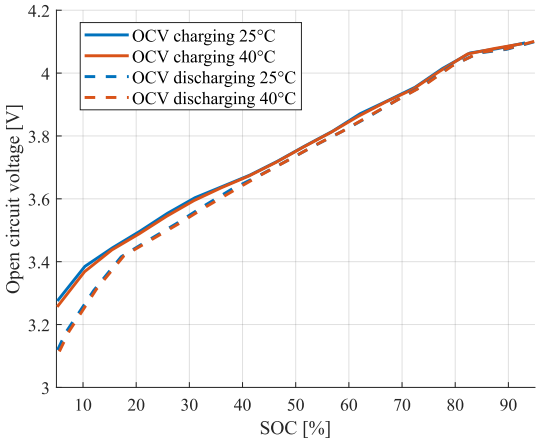

Fig. 4: OCV under different SOC and temperature.

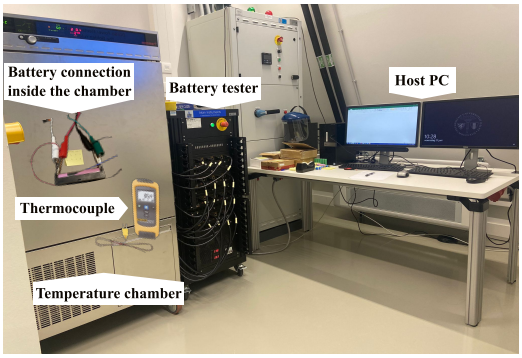

Fig. 5: Experiment setup for battery tests.

where

$$\begin{aligned} d = \big[&-1.1274 \times 10^{-13},\ 3.8095 \times 10^{-11}, \\ &-4.8269 \times 10^{-9},\ 2.8005 \times 10^{-7}, \\ &-7.0790 \times 10^{-6}, 5.2248 \times 10^{-5},\ 2.1565 \times 10^{-4}\big] \end{aligned} \tag{7}$$

and coefficient of determination (R^2) is 0.5257.

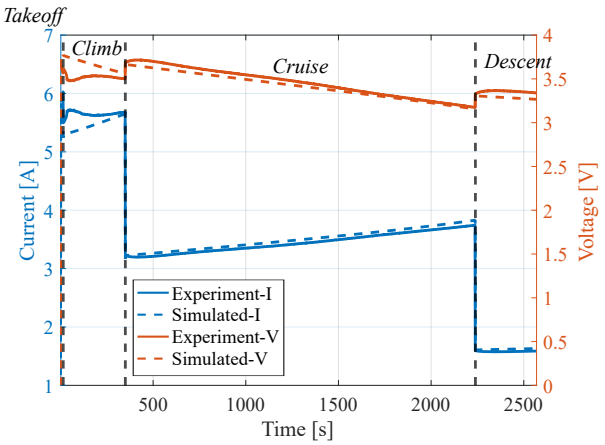

(a) Voltage and current profile.

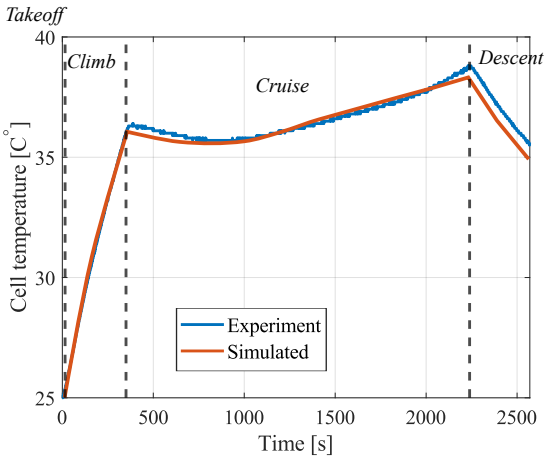

(b) Temperature profile.

Fig. 6: Experimental verification under specified AEA flight.

C. Experiment verification

To verify the proposed battery electro-thermal cell model, an experiment was conducted. Fig. 5 illustrates the experimental setup, which comprises a battery tester, a temperature chamber to regulate ambient temperature, a type-K temperature sensor to measure battery cell surface temperature, and a host PC for monitoring, controlling the test, and recording data. An example electric aircraft power profile from [6], including takeoff, climb, cruise, and descent, was normalized to the cell level and applied to the battery cell. The temperature chamber was set to $25°C$. The resulting simulated and experiment voltage-current and temperature data are shown in Fig. 6. For temperature prediction, the electro-thermal battery cell model achieved an MAE of 0.30, an RMSE of 0.24, and a coefficient of determination (R^2) of 0.9940, demonstrating its high accuracy and reliability.

III. Battery Sizing for All-Electric Aircraft

In the conventional fuel-based aircraft propulsion system, the propulsion of the aircraft is performed by the gas turbine engine, while jet fuel is the onboard energy source. For the AEA, the electric power sourced from the battery is transmitted to the electric motor, which drives the propeller or fan [11]. The transition to electric propulsion eliminates the need for fuel and engines, but it introduces additional weight due to the integration of the electric powertrain. Therefore, it is necessary to compute the weight difference between the conventional fuel-based aircraft and the retrofitted AEA to estimate the takeoff gross weight (TOGW) of the AEA. As expressed in (8), the TOGW of the retrofitted AEA W_{to} can be broken down into battery weight W_{b}, payload weight W_{pl}, and the modified OEW W_{oe}. The payload weight is assumed to be the same as that of the reference aircraft. Additionally, it is assumed that the transition to electric propulsion does not significantly affect the overall airframe design [12]. Therefore, the modified OEW of the AEA W_{oe} can be further decomposed as (9). The engine contribution W_{en} in the fuel-based aircraft is excluded, and the wing weight is considered separately.

$$W_{\text{to}} = W_{\text{b}} + W_{\text{pl}} + W_{\text{oe}} \tag{8}$$

$$W_{\text{oe}} = W_{\text{oe.ref}} - W_{\text{w.ref}} - W_{\text{en}} + W_{\text{PT}} + W_{\text{w}} \tag{9}$$

where $W_{\text{w.ref}}$ and W_{w} represent the wing weight of the reference aircraft and the retrofitted AEA, respectively. Both $W_{\text{w.ref}}$ and W_{w} are estimated using the empirical correlation described in [13]. The all-electric powertrain weight, W_{PT}, includes the DC/DC converter, DC/AC inverter, electric motor, gearbox, and associated cabling weights. These components are sized based on the takeoff power, as this phase has the highest power consumption. Their weights are subsequently determined using state-of-the-art power density value.

A. Power and energy requirements

A typical flight profile for a small aircraft consists of five distinct phases: takeoff, climb, cruise, descent, and landing. Furthermore, to accommodate unanticipated emergency flight operations, AEA batteries must include reserve energy as a safety margin [3], [4]. When sizing the battery pack for an AEA, the landing phase is neglected, as it requires significantly less power and consumes minimal energy [12]. Due to the relatively lower power and energy density requirements, a small aircraft capable of carrying four passengers is considered, and the reference aircraft is selected as the Cessna 172R. The lift coefficient, drag coefficient, and performance

indices are matched to those of the selected reference conventional aircraft [6]. To simplify the analysis, the transitional periods between flight phases are neglected [5].

First, the takeoff phase is typically characterized by Takeoff speed V_{to} and takeoff run length L_{to}, and these parameters can be estimated by evaluating the aircraft's acceleration along the runway based on horizontal force equilibrium. The forces involved in this process include the thrust, the friction, and the aerodynamic drag. Based on this, the takeoff time T_{to} can be determined, with the detailed calculations provided in [6]. In the climb, descent, cruise, and reserve phases, a general expression for the required power can be obtained based on the equilibrium of all the forces acting upon an aircraft [14].

$$P_{\text{i}} = W_{\text{to}} V^{\text{v}}_{\text{roi,i}} + \left(\frac{1}{2}\rho^{\text{i}} S V_{\text{i}}^3 C^{\text{i}}_{\text{D0}} + K^{\text{i}} \frac{W_{\text{to}}^2}{\frac{1}{2}\rho^{\text{i}} S V_{\text{i}}}\right) \tag{10}$$

where $V^{\text{v}}_{\text{roi,i}}$ represents the vertical velocity, ρ^{i} is the air density, V_{i} is the aircraft true airspeed. C^{i}_{D0} and K^{i} are the zero-lift drag coefficient and induced drag correction factor, respectively. The subscript roi and i denote each flight phase.

The total battery energy required for an AEA trip can be calculated by integrating the specific power required for each flight phase over time. The battery efficiency η_{b} is calculated based on the ECM in sec II-A.

$$\begin{aligned} P_{\text{i,b}} &= \frac{P_{\text{i}}}{\eta_{\text{conv}}\eta_{\text{inv}}\eta_{\text{cabl}}\eta_{\text{em}}\eta_{\text{gb}}\eta_{\text{prop}}} \\ \eta_b &= \frac{P_{\text{i,b}}}{P_{\text{i,b}} + I^2(R_{\text{o}} + R_{\text{s}} + R_{\text{l}})} \end{aligned} \tag{11}$$

where $P_{\text{i,b}}$ represents the power required by the powertrain from the battery pack. η_{x} represents the efficiency of each all-electric powertrain component.

B. Sizing result

Based on the electro-thermal battery cell model in Sec. II, mission performance requirement and aircraft specifications in [6], power and energy calculation in III-A, the relationship between weight components in (8), and battery efficiency calculation in eq. (11), the system encompassing W_{to}, W_{oe}, and W_{b} can be closed. An iterative calculation is performed to determine the TOGW and battery pack size of the retrofit AEA based on the reference Cessna 172R while adhering to a set of constraints to ensure the validity of the retrofit design, including the empty weight ratio, the wing loading, and the battery power constraints. Detailed discussion about the constraints can be found in [6].

TABLE II: Technical specifications of the retrofit AEA.

Model	Retrofit Cessna 172R
Range R	$118.50\,\text{km}$
Battery size E_{b}	$208.23\,\text{kW h}$
Battery pack mass M_{b}	$1062.40\,\text{kg}$
Operating empty mass M_{oe}	$865.37\,\text{kg}$
Takeoff mass M_{to}	$2272.65\,\text{kg}$
Wing loading $\frac{W_{\text{to}}}{S}$	$771.44\,\text{N m}^{-2}$
Power loading $\frac{P_{\text{peak}}}{W_{\text{to}}}$	$0.091\,\text{N W}^{-1}$
Empty weight fraction $\frac{W_{\text{oe}}}{W_{\text{to}}}$	0.38

This battery sizing procedure updates the battery efficiency and temperature every second, using the calculated resistance and current from the electrical and thermal functions based on the given aerodynamic power requirements. By integrating the energy over time and considering the partial weight in the AEA, the battery pack size and takeoff weight can be determined. The process iterates until the sizing results satisfy all constraints.

The sizing results for the retrofit Cessna 172 using the Samsung 35E battery with a packing efficiency of 0.8 are detailed in Tab. II. The maximum range achievable is $118.50\,\text{km}$, requiring a battery pack size of $208.23\,\text{kW h}$. The battery power and efficiency over the whole flight mission of the designed AEA at ambient temperature $25°C$ are shown in Fig. 7. It can be observed that due to the lower power requirement during the cruise and reserve phases, the battery efficiency is higher compared to the takeoff and climbing phases. However, during the reserve phase, the SOC becomes low, leading to increased battery cell resistance and, consequently, a significant drop in efficiency. Compared to the battery sizing method in [6], which assumes a constant battery efficiency of 96% and can achieve a maximum range of $133\,\text{km}$ with a battery pack size of $206.95\,\text{kW h}$ using the same battery cell type, the AEA sizing method using the electro-thermal battery cell model yields a maximum achievable range that is 10.9% lower due to the actual lower battery efficiency, with an average value of approximately 92.70% throughout the flight mission. This demonstrates that battery efficiency plays a crucial role in the AEA sizing outcome.

According to the discussion in Sec.II-A, high temperatures can lower the resistance at the same SOC and current conditions, thereby improving efficiency. Hence, the efficiency profile of the designed AEA under varying battery cell operating temperatures during the flight mission is shown in Fig. 8. The BTMS is assumed to function effectively, maintaining a constant cell ambient temperature throughout. It can be observed that

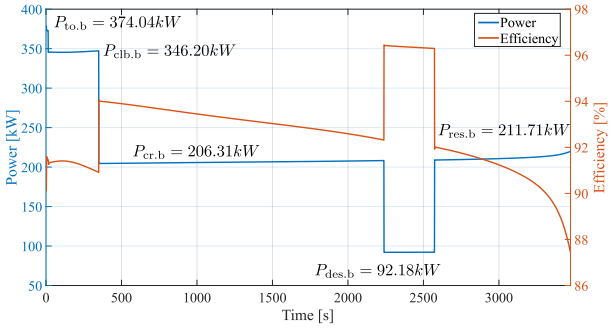

Fig. 7: Battery power and efficiency during the flight.

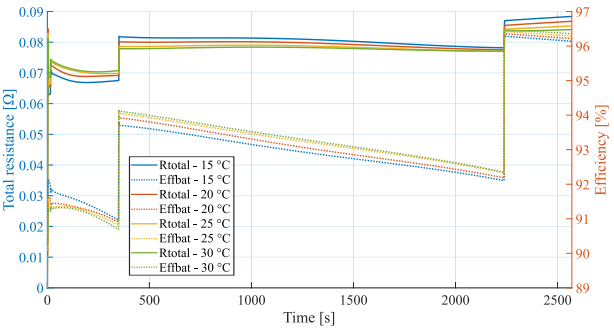

Fig. 8: Battery resistance and efficiency under different battery cell operating temperatures.

low temperatures lead to higher total resistance in the battery, resulting in a reduction in efficiency. The average efficiency throughout the entire flight mission is 92.74% at $30°C$ and 92.49% at $15°C$, respectively. Therefore, when designing the BTMS, it is advisable to moderately increase the target temperature to improve operational efficiency. However, this approach presents a trade-off, as higher temperatures can accelerate battery aging and lead to increased internal resistance over time.

IV. Conclusion

In conclusion, an electro-thermal battery cell model integrated sizing method for small, short-range AEAs, using a commercial aircraft as a reference, has been outlined. This method enables the determination of battery size for a 4-seater AEA based on specified top-level design parameters. It establishes an analytical relationship between power profiles across different flight phases, weight components contributing to takeoff weight, and a set of design constraints. Varying battery efficiency over the entire flight mission is considered based on an electro-thermal battery cell model. The battery efficiency observed under different ambient temperatures demonstrated that the BTMS can be designed to increase the target operating temperature to optimize battery cell performance while improving overall efficiency without compromising battery lifetime and safety.

References

[1] A. Schwab, A. Thomas, J. Bennett, E. Robertson, and S. Cary, "Electrification of aircraft: Challenges, barriers, and potential impacts," National Renewable Energy Laboratory, Tech. Rep., 10 2021. [Online]. Available: https://www.osti.gov/biblio/1827628

[2] Y. Liang, G. R. C. Mouli, and P. Bauer, "Charging technology for electric aircraft: State of the art, trends, and challenges," *IEEE Transactions on Transportation Electrification*, 2023.

[3] C. E. Riboldi and F. Gualdoni, "An integrated approach to the preliminary weight sizing of small electric aircraft," *Aerospace Science and Technology*, vol. 58, pp. 134–149, 2016.

[4] C. E. Riboldi, "An optimal approach to the preliminary design of small hybrid-electric aircraft," *Aerospace Science and Technology*, vol. 81, pp. 14–31, 2018.

[5] A. Bills, S. Sripad, W. L. Fredericks, M. Singh, and V. Viswanathan, "Performance metrics required of next-generation batteries to electrify commercial aircraft," *ACS Energy Letters*, vol. 5, no. 2, pp. 663–668, 2020.

[6] Y. Liang, D. Bodnár, G. R. C. Mouli, D. Ragni, and P. Bauer, "Charging demand prediction: Small all-electric aircraft and electric vertical takeoff and landing aircraft," *IEEE Transactions on Transportation Electrification*, 2024.

[7] L. Lam, P. Bauer, and E. Kelder, "A practical circuit-based model for li-ion battery cells in electric vehicle applications," in *2011 IEEE 33rd International Telecommunications Energy Conference (INTELEC)*, 2011, pp. 1–9.

[8] "Specification of product for lithium-ion rechargeable cell: INR18650-35E," Samsung SDI Co., Ltd. Battery Business Division, 2016. [Online]. Available: https://datasheet.octopart.com/INR18650-35E-Samsung-datasheet-103126726.pdf

[9] M. Muratori, M. Canova, and Y. Guezennec, "A spatially-reduced dynamic model for the thermal characterisation of li-ion battery cells," *International journal of vehicle design*, vol. 58, no. 2-4, pp. 134–158, 2012.

[10] Y. Xie, X. Wang, X. Hu, W. Li, Y. Zhang, and X. Lin, "An enhanced electro-thermal model for ev battery packs considering current distribution in parallel branches," *IEEE Transactions on Power Electronics*, vol. 37, no. 1, pp. 1027–1043, 2021.

[11] A. R. Gnadt, R. L. Speth, J. S. Sabnis, and S. R. Barrett, "Technical and environmental assessment of all-electric 180-passenger commercial aircraft," *Progress in Aerospace Sciences*, vol. 105, pp. 1–30, 2019.

[12] R. de Vries, M. T. Brown, and R. Vos, "A preliminary sizing method for hybrid-electric aircraft including aero-propulsive interaction effects," in *2018 aviation technology, integration, and operations conference*, 2018, p. 4228.

[13] D. Raymer, *Aircraft design: a conceptual approach*. American Institute of Aeronautics and Astronautics, Inc., 2012.

[14] J. D. Anderson and M. L. Bowden, *Introduction to flight Eighth edition*. McGraw-Hill Higher Education New York, NY, USA, 2016, vol. 582.